The Planetary Science Journal, 5:181 (11pp), 2024 August https://doi.org/10.3847/PSJ/ad5b5d

Contribution of the Moon-forming Impactor to the Volatile Inventory in the Bulk Silicate Earth

Damanveer S. Grewal[1,2], Yoshinori Miyazaki[3], and Nicole X. Nie[4]
[1] School of Molecular Sciences, Arizona State University, Tempe, AZ 85281, USA; damanveer.grewal@asu.edu
[2] School of Earth and Space Exploration, Arizona State University, Tempe, AZ 85281, USA
[3] Division of Geological and Planetary Sciences, California Institute of Technology, Pasadena, CA 91125, USA
[4] Department of Earth, Atmospheric, and Planetary Sciences, Massachusetts Institute of Technology, Cambridge, MA 02139, USA
Received 2024 May 11; revised 2024 June 17; accepted 2024 June 19; published 2024 August 23

Abstract

The timing and mechanism by which the present-day inventory of life-essential volatiles hydrogen–carbon–nitrogen–sulfur (H–C–N–S) in the bulk silicate Earth (BSE) was established are debated. In this study we have modeled the equilibrium partitioning of H–C–N–S between core, magma ocean (MO), and atmosphere to determine whether the Moon-forming impactor (MFI) was the primary source of volatiles in the BSE. Our findings suggest that the MFI's core and MO-degassed atmosphere were its primary H–C–N–S reservoirs. Since the MFI likely lost its MO-degassed atmosphere before the giant impact, most of the BSE's volatiles must come from the small fraction of the MFI's core which reequilibrated with Earth's post-impact MO. This implies a high H–C–N–S inventory in the MFI (up to 50% of volatile-rich carbonaceous chondrites) to establish the BSE's volatile budget. Although isotopic compositions of nonvolatile elements do not rule out the possibility of substantial volatile-rich, carbonaceous material accretion, MFI's collisional growth from thermally metamorphosed/differentiated planetesimals makes it improbable that it contained ∼50% carbonaceous chondrite equivalent of H–C–N during its differentiation. Therefore, the MFI was unlikely the primary source of volatiles in the BSE. A significant portion of the BSE's volatile inventory (especially H and C) likely predates the Moon-forming event. To prevent loss to space and segregation into Earth's core, volatile-bearing materials must be delivered during the final accretion event(s) preceding the Moon-forming event. The substantial size of the proto-Earth at this stage, combined with limited metal–silicate equilibration during the Moon-forming event, facilitated the retention of these volatiles within the BSE.

Unified Astronomy Thesaurus concepts: Planet formation (1241); Planetary science (1255); Meteorites (1038); Cosmochemistry (331); Earth atmosphere (437); Earth (planet) (439)

1. Introduction

The exchange of life-essential volatiles such as hydrogen (H), carbon (C), nitrogen (N), and sulfur (S) among the major reservoirs of the bulk silicate Earth (BSE = mantle + crust + hydrosphere + atmosphere) plays a critical role in defining the long-term habitability of our planet (Marty 2012; Hirschmann 2016). However, there is an ongoing debate regarding when the present-day inventory of volatiles in the BSE was established. Is the BSE volatile inventory a vestige of the entirety of Earth's growth, or was it established during the later stage, provided that the early-accreted volatiles efficiently segregated into its core or were lost to space during impacts (Albarède 2009; Marty 2012; Halliday 2013; Wang & Becker 2013; Hirschmann 2016; Braukmüller et al. 2019; Budde et al. 2019; Grewal et al. 2019b, 2021b, 2021c; Alexander 2022)? This uncertainty arises from two key factors: (1) Earth's protracted growth, which involved punctuated accretion of differentiated planetesimals and planetary embryos from different regions of the disk (Rubie et al. 2011; Dauphas 2017; Burkhardt et al. 2021; Gu et al. 2023); and (2) the atmophile and siderophile nature of H–C–N–S, which makes their inter-reservoir distribution highly sensitive to core–mantle differentiation and magma ocean (MO) degassing (Grewal et al. 2019a; Speelmanns et al. 2019; Grewal et al. 2020, 2021b; Jackson et al. 2021; Sakuraba et al. 2021; Grewal et al. 2022a; Shi et al. 2022; Li et al. 2023; Suer et al. 2023; Gu et al. 2024). The complex and stochastic nature of these processes makes it challenging to determine whether the present-day inventory of H–C–N–S in the BSE is a vestige of the entirety of Earth's growth or in line with the atmophile and siderophile character of these elements, biased toward the later stages of accretion.

In contrast to the considerable stochasticity during the earlier stages, the last stages of Earth's growth are better defined. The main phase of Earth's growth concluded with the Moon-forming giant impact between the proto-Earth and a Mars-sized impactor (referred to as the "canonical model" of Moon formation (Canup & Asphaug 2001; Canup 2004). Although more complex models on the giant impact have been recently proposed (Pahlevan & Stevenson 2007; Canup 2012; Cuk & Stewart 2012; Rufu et al. 2017), we focus on the more commonly accepted canonical model in this study. Additionally, a minor inventory of late accretion ($<0.004\,M_E$) following the giant impact is required to account for the abundances of highly siderophile elements in the BSE (Walker et al. 2015; Fischer-Gödde et al. 2020). Given the atmophile and siderophile character of H–C–N–S and their substantial depletion in the BSE compared to chondrites, late accretion (Wang & Becker 2013; Braukmüller et al. 2019) and, more recently, the Moon-forming impactor (MFI; Budde et al. 2019; Grewal et al. 2019b) have been alternately proposed as the primary source of volatiles in the BSE.

Considering that Earth did not experience any major accretion events after the Moon-forming giant impact, the idea of establishing the present-day inventory of volatiles in the BSE during late accretion is an appealing hypothesis. Previous research has suggested that late accretion could potentially account for nearly the entire inventory of S in the BSE (Wang & Becker 2013; Braukmüller et al. 2019). However, reductions in the estimated mass of late accretion, and the ambiguities related to its source reservoir (Walker et al. 2015; Fischer-Gödde & Kleine 2017; Fischer-Gödde et al. 2020), place limitations on its contribution to the present-day inventory of H–C–N–S in the BSE. For instance, based on the latest estimates by Alexander (2022), late accretion involving $\sim$0.0018 M_E of CM chondrites could deliver almost the entire inventory of N, $\sim$33% of the H and S, and $\sim$10% of the C in the BSE, and involving $\sim$0.0022 M_E of enstatite chondrites (ECs) would provide $\sim$25% of the inventory of N, $\sim$50% of the S, and $\sim$2% of the C in the BSE, but no H. The relative fractionation of H–C–N–S abundances in the BSE compared to chondrites (Hirschmann 2016; Dasgupta & Grewal 2019), along with the elemental and isotopic abundances of noble gases in the BSE (Marty 2012; Alexander 2022), also suggests that late accretion was not the primary source of the present-day inventory of volatiles in the BSE. Additionally, late accretion through differentiated impactor(s) (Bottke et al. 2010; Genda et al. 2017; Marchi et al. 2018), rather than chondrite-like primitive materials, would further restrict its contribution to the BSE inventory of highly volatile elements like H, C, and N. This constraint arises owing to the extensive volatile loss experienced by planetesimal-sized bodies during their differentiation (Hirschmann et al. 2021; Grewal et al. 2022a, 2022b; Grewal 2022; Grewal & Asimow 2023; Newcombe et al. 2023; Peterson et al. 2023a, 2023b; Grewal et al. 2024). Therefore, the majority of the present-day inventory of H–C–N–S in the BSE was likely established during the main phase of Earth's growth (Marty 2012; Alexander 2022).

Could the MFI be the primary source of the present-day inventory of H–C–N–S in the BSE? Given that the Moon-forming event marked the final major accretion event on Earth, it is worth investigating this possibility. Recent research, drawing on geochemical evidence, has suggested that the MFI could be the primary source of H–C–N–S in the BSE (Budde et al. 2019; Grewal et al. 2019b). For instance, Mo isotopes in Earth's mantle suggest that the final $\sim$10%–20% of Earth's accretion occurred through the accretion of a mixture of inner and outer solar system materials (noncarbonaceous (NC) and carbonaceous (CC), respectively; Budde et al. 2019). A substantial input of volatile-rich CC-reservoir-derived materials can aid in establishing the BSE volatile inventory during the Moon-forming event (Budde et al. 2019). Since the MFI was a differentiated object, the distribution of H–C–N–S between its core, mantle, and atmosphere dictates its contribution to the inventory of these elements in the BSE. Considering the partitioning of C–N–S between the MFI's mantle and core, Grewal et al. (2019b) demonstrated that a Mars-sized impactor could potentially establish the inventory of C–N–S in the BSE under specific conditions. These include the following: (1) the bulk silicate proto-Earth (hereafter BSp-E) was devoid of C, N, and S prior to the Moon-forming event; (2) the MFI's core was S-rich (>22 wt% S) and graphite saturated (meaning that the C content in the S-rich core exceeded its saturation limit for C, and the excess C was exsolved as graphite/diamond into the MFI's mantle); and (3) the MFI's core did not reequilibrate with the proto-Earth's mantle. However, the extent to which each of these unique conditions is met remains poorly understood.

Given the recent revisions in the inventory of C in the BSE (Marty et al. 2020), discoveries highlighting significant differences between the fO_2 of atmosphere–MO interaction and that of metal–silicate equilibration within deep MOs (Armstrong et al. 2019; Hirschmann 2022; Kuwahara et al. 2023), and advancements in our understanding of the metal/silicate partitioning behavior of H–C–N–S, especially under the extreme pressures–temperatures (P–T) relevant to deep MOs (Suer et al. 2017; Tagawa et al. 2021; Blanchard et al. 2022; Huang et al. 2024), it is now imperative to reevaluate the hypothesis concerning volatile delivery during the Moon-forming event. In this study, we model the equilibrium partitioning of H–C–N–S between atmosphere, MO, and core in the post-impact Earth and the MFI. These models are used in conjunction with geochemical constraints regarding the chemical composition of the MFI to quantify whether it was the primary source of H–C–N–S in the BSE.

2. The Fate of H–C–N–S in the Post–Giant Impact Earth

To assess whether the MFI alone can account for the present-day inventory of H–C–N–S in the BSE, we employ an inverse numerical approach. If the entire inventory of H–C–N–S in the BSE was delivered by the MFI, the BSp-E must have been H–C–N–S-free prior to the giant impact. Based on this assumption, any volatiles accreted to the proto-Earth before the giant impact were either segregated into its core or lost to space during atmospheric erosion. For this end-member scenario, the known inventory of H–C–N–S in the BSE is a constraint for the required H–C–N–S abundances in the MFI. After the giant impact, H–C–N–S delivered by the MFI were partitioned among the molten fraction of the BSp-E, the bulk silicate impactor (BSI), the impactor's core, and the degassed atmosphere, while the core of proto-Earth was isolated (Figure 1). The impactor's core would eventually sink into Earth's core.

2.1. Governing Mass Balance Equations for the Post-impact Equilibration on Earth

Following the approach of several studies on this topic (Kuramoto & Matsui 1996; Hirschmann 2016; Grewal et al. 2021b; Jackson et al. 2021; Sakuraba et al. 2021; Li et al. 2023; Gu et al. 2024), volatile exchange between the atmosphere, MO, and the metal phase in the post-impact Earth is quantified based on the chemical equilibrium between these reservoirs. Chemical equilibrium can be established if material exchange between the post-impact atmosphere, MO, and the metal phase is efficient. The material exchange between MO and the metal phase is efficient provided that the metallic droplets are small enough to allow for rapid equilibration (Stevenson 1990; Dahl & Stevenson 2010). The efficiency of material exchange among the metal phase, MO, and atmosphere depends on the residence time of metal droplets in the MO, which again is controlled by the metallic droplet size and MO convection timescale (Ikoma et al. 2018). Scaling laws based on experiments predict that MO convection is highly vigorous (Solomatov 2007), while theoretical studies show that the impactor's core can get emulsified within MO (Stevenson 1990;

A) *Impactor retained its MO-degassed atmopshere before the giant impact*

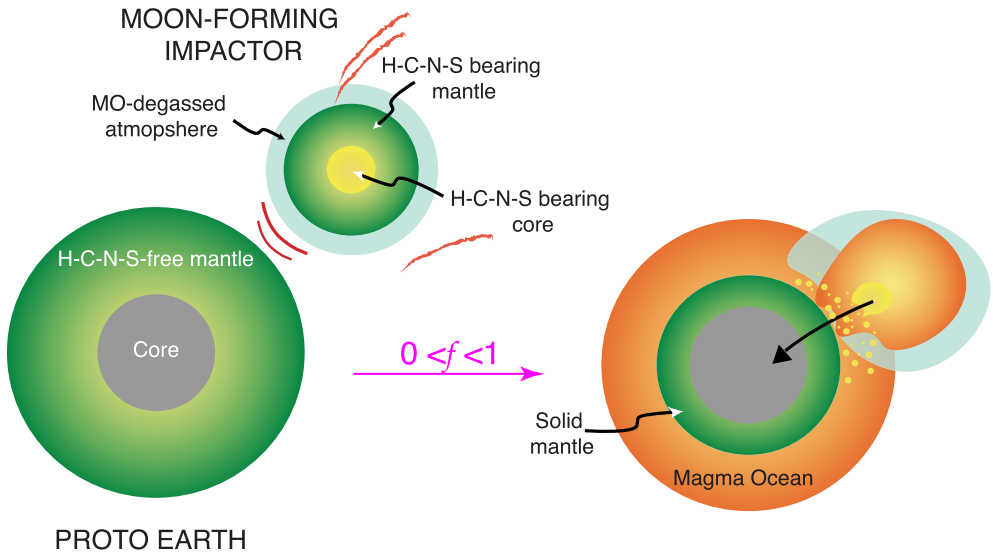

B) *Impactor lost its MO-degassed atmopshere before the giant impact*

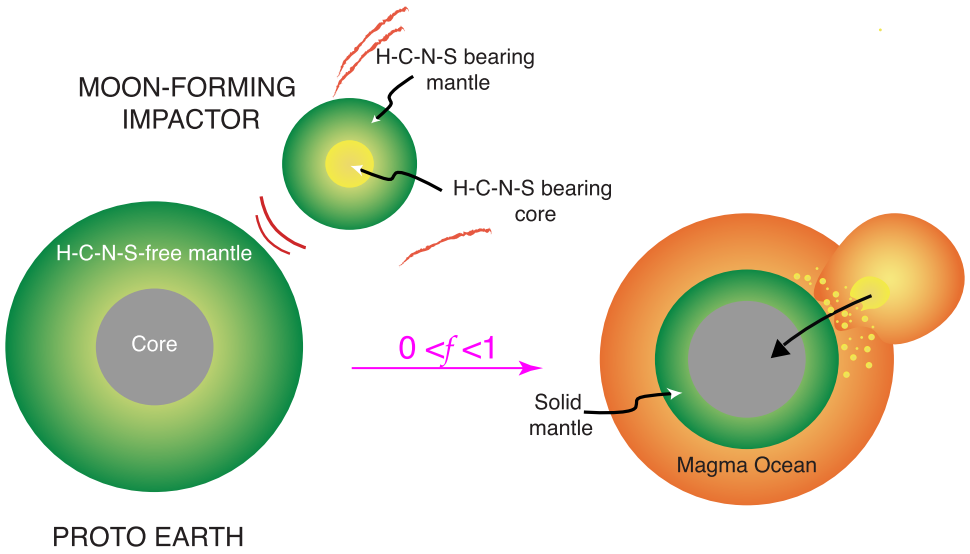

Figure 1. Illustration depicting the delivery of H–C–N–S to the proto-Earth exclusively by the MFI in cases where the impactor (a) retained or (b) lost its MO-degassed atmosphere before the giant impact. Post-impact, the inventory of H–C–N–S in the BSE is controlled by the exchange of these volatiles between the molten fraction of the mantle, the BSI (= mantle ± MO-degassed atmosphere), and the reequilibrating fraction of the impactor's core (f). Note that the BSp-E is H–C–N–S-free and the BSI and the impactor's core are H–C–N–S-bearing.

Dahl & Stevenson 2010), enabling chemical equilibrium between metallic droplets, MO, and atmosphere (Sossi et al. 2020; Young et al. 2023). Therefore, the total mass of a volatile element "i" participating in core, MO, and atmosphere equilibration in the post-impact Earth can be quantified using the following mass balance equation:

$$m_i^{\text{total}} = m_i^{\text{atm}} + m_i^{\text{MO}} + m_i^{\text{core,imp}} \quad (1)$$

Here "m" represents the mass of an element "i" in a given reservoir, the superscripts "atm" and "MO" denote the post-impact atmosphere and MO on Earth, respectively, and superscript "core,imp" denotes the impactor's core.

Equation (1) implicitly assumes that the entire impactor's core fragmented down to centimeter-scale metallic droplets, which efficiently equilibrate with the post-impact MO. However, this assumption does not hold for the cores of large impactors during giant impacts. Fluid dynamics models, laboratory experiments, and geochemical models predict that efficient fragmentation and complete chemical equilibration are not possible during giant impacts for 100–1000 km sized cores

Table 1
Constraints and Parameters Used in the Models

	BSE Conc. (μg g^{-1})	Post-impact Earth's MO		Impactor's MO	
		$D^{metal/silicate}$	S (μg g^{-1} MPa^{-1})	$D^{metal/silicate}$	S (μg g^{-1} MPa^{-1})
H	79 ± 10	50	see text	10	5
C	453 ± 70	100	1.6	1000, 100	0.55
N	2.8 ± 0.6	5	1	80, 30	1
S	225 ± 25	5	5000	100	5000
		P = 50–60 GPa T = 3500–4000 K fO_2 of metal–MO equilibration = IW – 2 fO_2 of atm–MO equilibration = IW to +0.5		P = 20 GPa T = 2000 K fO_2 of metal–MO equilibration = IW – 1.5 fO_2 of atm–MO equilibration = IW – 1	

Note. See the main text for details and relevant references.

in large impactors (Dahl & Stevenson 2010; Rudge et al. 2010; Deguen et al. 2014; Landeau et al. 2016). The majority of the impactor's core sinks directly through the mantle of the proto-Earth as large blobs (>10 km in diameter), and only a small portion fragments within the turbulent thermal zone to facilitate metal–silicate equilibration (Lherm & Deguen 2018; Landeau et al. 2021). To account for incomplete reequilibration of the impactor's core with the post-impact MO, we introduce a parameter f, which represents the fraction of the impactor's core that completely reequilibrates with the post-impact MO, while the remaining fraction $(1 - f)$ merges with the proto-Earth's core without reequilibration:

$$m_i^{total} = m_i^{atm} + m_i^{MO} + f \cdot m_i^{core,imp} \quad (2)$$

Note that the total mass of an element participating in the post-impact atmosphere, MO, and core equilibration, denoted as "m_i^{total}," is analogous to the total mass of that element present in the impactor, excluding the core fraction $(1 - f)$ that does not reequilibrate with the post-impact MO.

Since the entire volatile inventory of the BSE is assumed to be established during the Moon-forming event, the mass of an element in the post-impact atmosphere + MO is equal to its mass in the BSE, which results in

$$m_i^{atm} + m_i^{MO} = m_i^{BSE} \quad (3)$$

Therefore, Equation (2) can be rewritten as

$$m_i^{total} = m_i^{BSE} + f \cdot m_i^{core,imp} \quad (4)$$

m_i^{total} can further be expanded as

$$m_i^{total} = m_i^{BSE} + f.C_i^{core} \cdot M^{core,imp} \quad (5)$$

Here C_i^{core} represents the concentration of an element in the reequilibrating fraction of the impactor's core after its interaction with the post-impact MO on Earth, and $M^{core,imp}$ is the mass of the impactor's core.

The exchange of an element between the impactor's core and the post-impact MO is controlled by its equilibrium partition coefficient between metallic and silicate melt ($D_i^{metal/silicate}$), represented as

$$D_i^{metal/silicate} = C_i^{core}/C_i^{MO} \quad (6)$$

Substituting Equation (6) into Equation (5), we get

$$m_i^{total} = m_i^{BSE} + f.D_i^{metal/silicate}.C_i^{MO}.M^{core,imp} \quad (7)$$

Equation (7) involves two unknowns, m_i^{total} and C_i^{MO}. To replace the C_i^{MO} term in Equation (7), we can refer back to the two terms in Equation (3), m_i^{atm} and m_i^{MO}. These terms are related by the equilibrium between the atmosphere and the underlying MO, usually quantified using a simplified solubility relationship in the form of Henry's law:

$$C_i^{MO} = S_i.p_i \quad (8)$$

Here S_i represents the Henrian constant for an element, and p_i is the partial vapor pressure of the gaseous species of that element. The partial vapor pressure term is related to the mass of the vapor species in the atmosphere by

$$p_i = (m_i^{atm}.g^{Earth}.k_i.\mu/\mu_i)/A^{Earth} \quad (9)$$

Here k_i is a mass factor that corrects for the difference between the mass of element "i" in the atmosphere and the mass of its gaseous species. Parameters g and A represent the gravitational constant and the surface area of Earth, respectively. The factor μ/μ_i denotes the molar mass ratio of the average atmosphere and the gaseous species of element i.

By substituting Equations (8) and (9) into Equation (3), we obtain

$$(C_i^{MO}.A^{Earth})/(S_i.g^{Earth}.k_i.\mu/\mu_i) + m_i^{MO} = m_i^{BSE} \quad (10)$$

Equation (10) can be rearranged as follows:

$$C_i^{MO} = m_i^{BSE}/[(A^{Earth}/S_i.g^{Earth}.k_i.\mu/\mu_i) + M^{MO}] \quad (11)$$

Substituting C_i^{MO} into Equation (7), we arrive at Equation (12), which contains only one unknown, m_i^{total}:

$$m_i^{total} = m_i^{BSE} + f.D_i^{metal/silicate}.M^{core,imp}.m_i^{BSE}/[A^{Earth}/(S_i.g^{Earth}.k_i.\mu/\mu_i) + M^{MO}] \quad (12)$$

2.2. Parameter Values for Post-impact Equilibration on Earth

Among the variables on the right-hand side of Equation (12), the mass of a volatile element in the BSE (m_i^{BSE}) is directly determined through geochemical analysis. The mean inventories of H (79 ± 10 μg g^{-1}; Hirschmann 2018), N (2.8 ± 0.6 μg g^{-1}; Hirschmann 2018), and S (225 ± 25 μg g^{-1}; Hirschmann 2016) in the BSE are widely accepted in the

geochemical community (Table 1). However, the inventory of C in the BSE is a subject of debate, primarily due to discrepancies in the estimated abundance of C in Earth's mantle. Using the CO_2/Ba ratio of minimally degassed oceanic basalts from the convecting mantle, Hirschmann (2018) estimated the C inventory in the BSE to be $140 \pm 40\ \mu g\ g^{-1}$. In contrast, Marty et al. (2020), using the C/N ratios of mantle-derived CO_2-rich gases, revised the mean C inventory of the BSE to $453 \pm 70\ \mu g\ g^{-1}$. Recent studies indicate that the CO_2/Ba ratios of both the upper and lower mantle are higher than previously reported (Shimizu et al. 2023; Sun & Dasgupta 2023). This suggests that the inventory of C in Earth's mantle is likely closer to the estimate of Marty et al. (2020). Therefore, we use the mean inventory of C in the BSE reported by Marty et al. (2020) in our models.

The values corresponding to the other parameters on the right-hand side of Equation (12) determined from numerical models and experimental data are outlined below and are reported in Table 1. Although uncertainties persist regarding the following parameters, in agreement with several previous studies on similar topics (e.g., Hirschmann 2016; Speelmanns et al. 2019; Jackson et al. 2021; Alexander 2022; Shi et al. 2022; Li et al. 2023), we do not aim to provide a comprehensive estimation of uncertainties, due to the exploratory nature of our models and the lack of realistic uncertainties for some parameters. Instead, our focus is on determining whether the MFI, as envisaged in the prevailing canonical model of planet formation, is capable on its own of supplying the present-day inventory of volatiles in the BSE. Our choice of parameters explores a most optimistic scenario for volatile delivery by the MFI.

1. *Mass of the impactor's core* ($M^{\mathrm{core,imp}}$): This parameter's value is determined by the core/mantle mass ratio of the canonical Mars-sized impactor ($0.1\,M_{\mathrm{E}}$; Canup & Asphaug 2001), which directly correlates with its oxygen fugacity (fO_2). State-of-the-art models of Earth's accretion and core formation track its fO_2 evolution by integrating growth histories derived from *N*-body simulations and determining the distribution of elements between metal and silicate following each impact to reproduce the abundances of several major and minor elements (e.g., Fe, Ni, Co, Nb, and Ta) in the BSE (Rubie et al. 2015; Fischer et al. 2017; Gu et al. 2023). These models indicate that the later stage of Earth's growth involved the accretion of oxidized planetary embryos ($\log fO_2 = \mathrm{IW} - 1.5$) from beyond 2 au. An fO_2 of IW − 1.5 for the oxidized planetary embryos in these models is identical to the fO_2 of Mars's accretion (Brennan et al. 2020). Consequently, the core/mantle mass ratio of the impactor was assumed to resemble that of Mars, i.e., $M^{\mathrm{core,imp}} = 0.025\ M_{\mathrm{E}}$, and is consistent with the prescribed values in Earth's accretion models.
2. *Degree of reequilibration of the impactor's core with the post-impact MO (f)*: Smoothed particle hydrodynamics (SPH) simulations and geochemical models suggest that nearly the entire core of the MFI directly crashed into the proto-Earth's core during the giant impact (Rudge et al. 2010; Piet et al. 2017; Zhou et al. 2022). The extent of core reequilibration during giant impacts has been investigated through theoretical studies and fluid dynamics experiments (Dahl & Stevenson 2010; Deguen et al. 2011, 2014; Landeau et al. 2021). Using this framework, Landeau et al. (2021) predicted that ∼7% of the impactor's core effectively reequilibrated with the post-impact MO for a canonical MFI. This small degree of reequilibration is also necessary for reproducing the abundances of siderophile elements, including Ni and Co, in the BSE (Fischer et al. 2015). Accordingly, we opt for a conservative estimate of $f = 0.1$ to account for the limited chemical exchange between the MFI's core and the post-impact MO. Note that the findings of this study are not significantly affected by the specific value of f used in the models. To demonstrate this, we examined lower and higher values of f, namely 0.05 and 0.2, respectively. Additionally, we present results for a notably high f value of 0.5, which is considered relatively unrealistic for the extent of reequilibration of the MFI's core.
3. *Mass of the post-impact MO on Earth (M^{MO})*: In Earth's accretion models, the mass of the target's mantle melted during giant impacts is calculated using melt-scaling laws (Nakajima et al. 2020). These laws parameterize outputs from hydrodynamic simulations to estimate the extent of melting in the target's mantle. Gu et al. (2023) used the melt-scaling laws of Nakajima et al. (2020) and determined extensive melting (half or more) of Earth's mantle after the canonical giant impact. The large degree of melting is consistent with predictions from geochemical models, which suggest metal–silicate equilibration in a deep MO (P = 50–60 GPa) to explain the Ni and Co abundances in the BSE (Wade & Wood 2005; Fischer et al. 2015). The extent to which a half-to-whole-mantle-scale MO fully engages in metal–silicate equilibrium remains a topic of debate. Therefore, we employ two extreme values for M^{MO}, namely $0.5M^{\mathrm{BSE}}$ and M^{BSE}, to accommodate the uncertainty surrounding the process of metal–silicate equilibrium following a giant impact. We note that if the mass of the post-impact MO equilibrating with the impactor's core was significantly lower than the above values (e.g., Deguen et al. 2011, 2014), the MFI's contribution to the volatile inventory of the BSE would be substantially lower than the upper bounds examined in this study.
4. *Metal/silicate partition coefficient* ($D_i^{\mathrm{metal/silicate}}$): The relevant $D_i^{\mathrm{metal/silicate}}$ values are determined using the parameterized equations from previous high pressure–temperature (P–T) experimental studies. These parameterized equations primarily depend on P, T, and fO_2. Recent Earth's accretion and core models, based on growth histories derived from *N*-body simulations, suggest that the geochemical composition of the BSE is most consistent with metal–silicate equilibration occurring at P = 50–60 GPa, T = 3500–4000 K, and $fO_2 = \mathrm{IW} - 2$ (Gu et al. 2023). These P–T–fO_2 values are well within the range of several geochemical models that track the fate of volatiles during the entire growth of Earth (Grewal et al. 2019a; Speelmanns et al. 2019; Jackson et al. 2021; Shi et al. 2022; Li et al. 2023; Gu et al. 2024). We used $D_i^{\mathrm{metal/silicate}}$ parameterized equations that incorporate experimental data collected at extreme P–T conditions. The relevant $D_i^{\mathrm{metal/silicate}}$ values, which are pertinent to the final core–mantle differentiation event on Earth, are as follows: $D_{\mathrm{H}}^{\mathrm{metal/silicate}} = 50$ (Tagawa et al. 2021), $D_{\mathrm{C}}^{\mathrm{metal/silicate}} = 250$ (Blanchard et al. 2022),

$D_N^{metal/silicate} = 5$ (Huang et al. 2024), and $D_S^{metal/silicate} = 5$ (Suer et al. 2017) (Table 1). Note that we chose to use the parameterization equation of Blanchard et al. (2022) over Fischer et al. (2020) to determine the relevant $D_C^{metal/silicate}$ value, due to concerns arising from C measurements within the silicate glasses in the latter study. The widespread presence of nanoscale metallic blebs throughout the silicate glasses likely compromised their experimental $D_C^{metal/silicate}$ values (Grewal et al. 2021a; Blanchard et al. 2022). As for $D_H^{metal/silicate}$, we decided against using the parameterized equations of Clesi et al. (2018) and Malavergne et al. (2019) because their H measurements in the metallic alloys were likely compromised owing to the decomposition of FeH_x, and resulting H escape, during the decompression of their experimental products (Tagawa et al. 2021). The $D_i^{metal/silicate}$ values for H, C, N, and S used in this study are similar to those used in a recent study for metal–silicate equilibration in the post–giant impact MO (Gu et al. 2023).

5. *Henrian solubility coefficient* (S_i): This is also an experimentally derived parameter and depends on fO_2, which governs the fugacity of its volatile vapor component and its speciation in the silicate melt (Hirschmann 2016). However, the fO_2 of metal–silicate equilibration cannot be directly applied to atmosphere–MO equilibration, due to vertical fO_2 gradients within deep MOs. These gradients result in the surface being more oxidized (IW to IW + 0.5) than the deeper layers, which equilibrate with the metal at IW − 2 (Sossi et al. 2020; Hirschmann 2022). For this fO_2 range, the adopted S_i values for C, N, and S are $S_C = 1.6\ \mu g\ g^{-1}\ MPa^{-1}$ for C dissolved as CO_3^{2-} (Hirschmann 2016), $S_N = 1\ \mu g\ g^{-1}\ MPa^{-1}$ for N dissolved as N_2 (Grewal et al. 2021b), and $S_S = 5000\ \mu g\ g^{-1}\ MPa^{-1}$ for S dissolved as all possible sulfurous species like S_2 and H_2S (Hirschmann 2016) (Table 1). Hydrogen mainly dissolves into the silicate melts in the form of molecular water (H_2O) and hydroxyl (OH^-) group at IW + 1, with molecular H_2 being the minor species (Stolper 1982; Sossi et al. 2023). Based on experimental data at 1 bar, the combined H_2O and OH^- solubility is proportional to $(fH_2O)^{0.5}$, indicating that a simple Henrian relationship is inadequate (Sossi et al. 2023). Therefore, we used a H_2O solubility relationship in the form of $\alpha.(fH_2O)^{0.5}$ to determine the H solubility in the MO (Table 1). An updated α value of $6470\ \mu g\ g^{-1}\ MPa^{-1}$ for peridotite-like silicate glasses was used in this study (Sossi et al. 2023).

2.3. Mass of H–C–N–S Involved in the Post-impact Atmosphere–MO Equilibration on Earth

In this subsection, we employ Equation (12) to determine the mass of each volatile element involved in the post-impact atmosphere–MO–core equilibration on Earth (m_i^{total}). These values will serve as constraints in Sections 3 and 4 to determine the volatile budget of the MFI, with the goal of establishing the present-day volatile inventory of the BSE. For the scenario with $f = 0.1$ and $M^{MO} = 0.5M^{BSE}$, the calculated values are as follows: $m_H^{total} = 1.4 \times m_H^{BSE}$, $m_C^{total} = 1.4 \times m_C^{BSE}$, $m_N^{total} = 1.0 \times m_N^{BSE}$, and $m_S^{total} = 1.0 \times m_S^{BSE}$ (Figure 2). Variation in f between 0.05 and 0.2 leads to small changes in m_H^{total} (1.2–1.8 $\times m_H^{BSE}$) and m_C^{total} (1.2–1.7 $\times m_C^{BSE}$), whereas for $f = 0.5$, m_H^{total} (3.0 $\times m_H^{BSE}$) and m_C^{total} (2.8 $\times m_C^{BSE}$) are considerably higher. m_N^{total} and m_S^{total} remain virtually unchanged with variations in f values. These variations in m_H^{total}, m_C^{total}, m_N^{total}, and m_S^{total} values with f can be attributed to the differences in their respective $D_i^{metal/silicate}$ and S_i values. Equation (12) demonstrates that m_i^{bulk} positively correlates with $D_i^{metal/silicate}$ and S_i. However, the impact of $D_i^{metal/silicate}$ is more significant than that of S_i. For instance, despite S_C ($1.6\ \mu g\ g^{-1}\ MPa^{-1}$) being considerably lower than S_S ($5000\ \mu g\ g^{-1}\ MPa^{-1}$), the variations in m_C^{bulk} with f are noticeably pronounced, due to the substantially higher $D_C^{metal/silicate}$ (250) compared to $D_S^{metal/silicate}$ (5). When compared to the scenario with $M^{MO} = 0.5M^{BSE}$ and $f = 0.1$, the values of m_H^{total} (1.2 $\times m_H^{BSE}$), m_C^{total} (1.3 $\times m_C^{BSE}$), m_N^{total} (1.0 $\times m_N^{BSE}$), and m_S^{total} (1.0 $\times m_S^{BSE}$) for the scenario with $M^{MO} = M^{BSE}$ and $f = 0.1$ show no substantial difference (Figure 2).

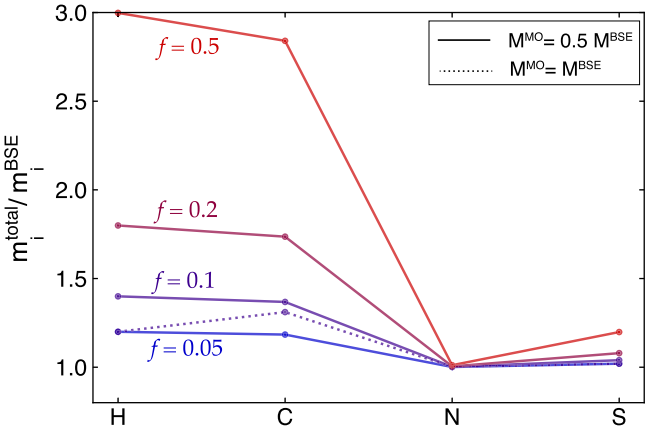

Figure 2. The total mass of an element participating in atmosphere–MO–core equilibration in the post–giant impact Earth (m_i^{total}) normalized to the mass of that element in the BSE (m_i^{BSE}). Within the realistic range of f values explored in this study ($f = 0.05$–0.2), m_i^{total} values lie in a narrow range, whereas for $f = 0.5$, m_i^{total} values for H and C are substantially higher.

3. Required Inventory of H–C–N–S in the MFI to Explain Their BSE Inventory

Now, with the values of total amount of a volatile element involved in post-impact atmosphere–MO–core equilibration (m_i^{total}) derived from Equation (12) in Section 2.3, we can determine the mass of volatiles required to be present in the whole MFI ($m_i^{whole,imp}$) in order to establish their inventory in the BSE (Figure 1(a)).

3.1. Governing Mass Balance Equations for Atmosphere–MO Equilibration in the MFI

The distribution of H–C–N–S within the whole MFI during its differentiation can be calculated using a mass balance equation similar to Equation (1):

$$m_i^{whole,imp} = m_i^{atm,imp} + m_i^{MO,imp} + m_i^{core,imp} \quad (13)$$

Since planetary embryos likely underwent almost complete metal–silicate equilibration (Dauphas & Pourmand 2011; Brennan et al. 2020), unlike Equation (2), the f parameter is not incorporated in Equation (13). Similar to the post-impact equilibration on Earth, the masses of an element in the MFI's

atmosphere ($m_i^{\mathrm{atm,imp}}$) and MO ($m_i^{\mathrm{MO,imp}}$) are related by S_i, and those in the MO ($m_i^{\mathrm{MO,imp}}$) and core ($m_i^{\mathrm{core,imp}}$) are related by $D_i^{\mathrm{metal/silicate}}$. However, the equilibration between the MFI's atmosphere and MO occurred at lower fO_2 and between its MO and core at lower P–T, compared to the post-impact Earth calculations in Section 2. The canonical MFI had the same mass and likely differentiated at a similar fO_2 to that of Mars (Rubie et al. 2015; Fischer et al. 2017; Gu et al. 2023). Consequently, we adopt the P–T–fO_2 conditions reported for differentiation of Mars for the MFI's differentiation (P = 20 GPa, T = 2000 K, and logfO_2 = IW − 1.5; Brennan et al. 2020; Table 1). The $D_i^{\mathrm{metal/silicate}}$ values under these conditions are $D_{\mathrm{H}}^{\mathrm{metal/silicate}}$ = 40 (Tagawa et al. 2021); $D_{\mathrm{C}}^{\mathrm{metal/silicate}}$ = 1000 and 100 for S-poor (<15wt% S) and S-rich (>15wt% S) cores, respectively (Tsuno et al. 2018); $D_{\mathrm{N}}^{\mathrm{metal/silicate}}$ = 80 and 30 for S-poor and S-rich cores, respectively (Grewal et al. 2021b); and $D_{\mathrm{S}}^{\mathrm{metal/silicate}}$ = 100 (Boujibar et al. 2014; Table 1). Note that the two end-member $D_{\mathrm{C}}^{\mathrm{metal/silicate}}$ and $D_{\mathrm{N}}^{\mathrm{metal/silicate}}$ values are used to account for the effect of S content in the core. This is because S is a major light element in the Martian core (Brennan et al. 2020; Khan et al. 2022) and could be present in substantial quantities in the core of the MFI (Li et al. 2016; Tsuno et al. 2018; Grewal et al. 2019b). The effect of S on $D_{\mathrm{H}}^{\mathrm{metal/silicate}}$ is currently unknown. The adopted S_i values for H, C, N, and S at IW − 1 (based on the fO_2 estimate for the surface of the Martian MO, which equilibrates with the metal at IW − 1.5 at depth; Hirschmann 2022) are $S_{\mathrm{H}} = 5\ \mu\mathrm{g\ g^{-1}\ MPa^{-1}}$ for H dissolved as H_2 (Sossi et al. 2023), $S_{\mathrm{C}} = 0.55\ \mu\mathrm{g\ g^{-1}\ MPa^{-1}}$ for C dissolved as CO (Hirschmann 2016), $S_{\mathrm{N}} = 1\ \mu\mathrm{g\ g^{-1}\ MPa^{-1}}$ for N dissolved as N_2 (Grewal et al. 2021b), and $S_{\mathrm{S}} = 5000\ \mu\mathrm{g\ g^{-1}\ MPa^{-1}}$ for S dissolved as all possible sulfurous species like S_2 and H_2S (Hirschmann 2016; Table 1).

In addition to $D_{\mathrm{C}}^{\mathrm{metal/silicate}}$, we must account for the solubility limit of C in the core ($C_{\mathrm{solubility}}$). This limit is heavily influenced by the S content of the core (Li et al. 2016; Tsuno et al. 2018; Grewal et al. 2019b; Hakim et al. 2019; Li et al. 2023) and can be a crucial factor in estimating the required C content in the MFI. The activity coefficient of C in the metal increases with increasing S content, resulting in a decrease in $C_{\mathrm{solubility}}$ (Wang et al. 1991; Bouchard & Bale 1995). Therefore, S-rich cores have lower $C_{\mathrm{solubility}}$ than S-poor cores (Li et al. 2016; Tsuno et al. 2018; Grewal et al. 2019b). If $C_{\mathrm{solubility}}$ is greater than the C content in the core predicted by $D_{\mathrm{C}}^{\mathrm{metal/silicate}}$, then $D_{\mathrm{C}}^{\mathrm{metal/silicate}}$ alone determines the C content of the core. However, if $C_{\mathrm{solubility}}$ is lower than the C content in the core predicted by $D_{\mathrm{C}}^{\mathrm{metal/silicate}}$, then $C_{\mathrm{solubility}}$ determines the C content in the core. The excess C, i.e., the difference between the C content in the core predicted by $D_{\mathrm{C}}^{\mathrm{metal/silicate}}$ and $C_{\mathrm{solubility}}$, is exsolved as graphite/diamond into the MO and provides an additional contribution to the inventory of C in the impactor's MO. We adopt the $C_{\mathrm{solubility}}$ obtained by Tsuno et al. (2018) in our models.

3.2. Required H–C–N–S Inventory of the MFI to Establish the Volatile Inventory in the BSE

Combining Equations (12) and (13), the required inventory of H–C–N–S in the whole MFI for the f = 0.1 and $M^{\mathrm{MO}} = 0.5M^{\mathrm{BSE}}$ scenario is $C_{\mathrm{H}}^{\mathrm{whole,imp}}$ = 0.19 wt%, $C_{\mathrm{C}}^{\mathrm{whole,imp}}$ = 1.34 wt%, $C_{\mathrm{N}}^{\mathrm{whole,imp}}$ = 0.002 1 wt%, and $C_{\mathrm{S}}^{\mathrm{whole,imp}}$ = 1.24 wt%

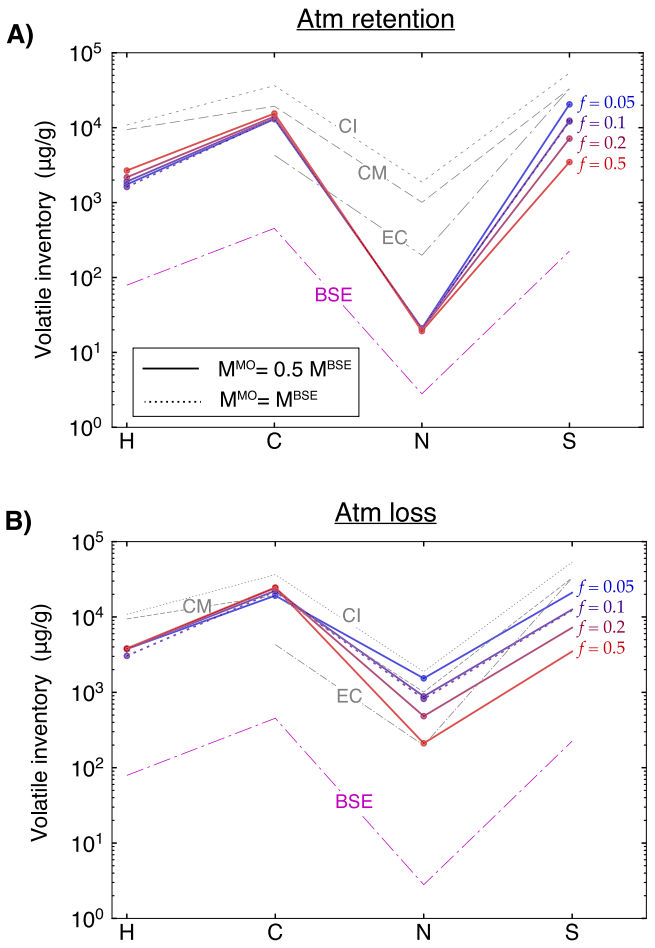

Figure 3. Required inventory of H–C–N–S in the MFI to establish the abundances of these elements in the BSE in cases where the impactor (a) retained or (b) lost its MO-degassed atmosphere before the giant impact. In panel (a) MFI is required to contain subchondritic content of H, C (except for ECs), N, and S, whereas in panel (b) the required inventories of N and C fall between those of ECs and CIs/CMs and the required inventories of H and S are lower than those of chondrites (except for ECs, which are almost H-free). H–C–N–S inventories in the BSE (Hirschmann 2018; Marty et al. 2020) and in EC, CM, and CI chondrites (Alexander 2022) are also plotted for comparison.

(Figure 3(a)). The required inventories of H (except for ECs, which are almost H-free; Alexander 2022), N, and S in the MFI are subchondritic, whereas that of C is intermediate between ECs and CIs/CMs. Since the MFI's core is not S-rich (3.7 wt% S; Figure 4), $D_{\mathrm{C}}^{\mathrm{metal/silicate}}$ and $D_{\mathrm{N}}^{\mathrm{metal/silicate}}$ values for S-poor cores are applicable. The C content in the core predicted by $D_{\mathrm{C}}^{\mathrm{metal/silicate}}$ is lower than $C_{\mathrm{solubility}}$. Consequently, C content in the core and MO was governed solely by $D_{\mathrm{C}}^{\mathrm{metal/silicate}}$. The majority of N (80%) in the MFI resides in its MO-degassed atmosphere, whereas the majority of H (70%), C (75%), and S (99%) reside in its core (Figure 5). Variation in f between 0.05 and 0.5 leads to small changes in $C_{\mathrm{H}}^{\mathrm{whole,imp}}$ (0.17–0.27 wt%), $C_{\mathrm{C}}^{\mathrm{whole,imp}}$ (1.30–1.55 wt%), and $C_{\mathrm{N}}^{\mathrm{whole,imp}}$ (0.0019–0.0020 wt%) values, whereas the variation in $C_{\mathrm{S}}^{\mathrm{whole,imp}}$ (0.35–2.05 wt%) values is considerably higher (Figure 3(a)). For the scenario with $M^{\mathrm{MO}} = M^{\mathrm{BSE}}$ and f = 0.1, the values of $C_{\mathrm{H}}^{\mathrm{whole,imp}}$ (0.16 wt%), $C_{\mathrm{C}}^{\mathrm{whole,imp}}$ (1.32 wt%), $C_{\mathrm{N}}^{\mathrm{whole,imp}}$ (0.0021 wt%), and $C_{\mathrm{S}}^{\mathrm{whole,imp}}$ (1.21 wt%) are almost identical to the scenario with $M^{\mathrm{MO}} = 0.5M^{\mathrm{BSE}}$ and f = 0.1.

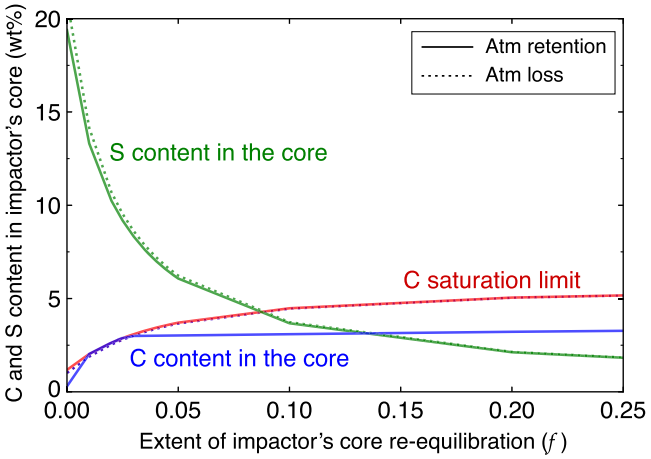

Figure 4. Comparison between the S content in the impactor's core, its C content predicted by $D_C^{metal/silicate}$, and its graphite-saturated C solubility limit ($C_{solubility}$) as a function of the extent of its reequilibration with the post-impact MO (f). In the case of the impactor retaining its MO-degassed atmosphere prior to the Moon-forming giant impact, C content in the core predicted by $D_C^{metal/silicate}$ is generally lower than $C_{solubility}$, except for a narrow range of f. This means that the MFI's core was almost always C undersaturated for the atmospheric retention case, whereas for the case of atmospheric loss before the impact, the impactor's core is C saturated for almost all values of f.

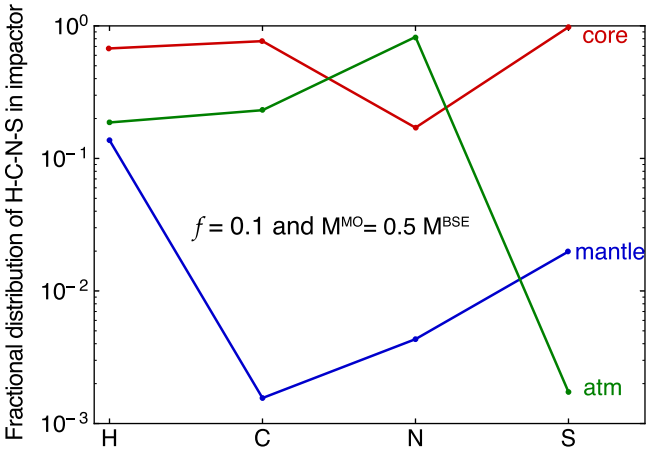

Figure 5. H–C–N–S distribution between the core, MO, and MO-degassed atmosphere of the MFI for the $f = 0.1$ and $M^{MO} = 0.5M^{BSE}$ scenario. The MO-degassed atmosphere is the major N reservoir, but it also contains a substantial amount of C and H, whereas the impactor's core is the major H, C, and S reservoir. Similar distribution patterns are applicable for the other scenarios explored in this study.

4. Effect of the Loss of MFI's MO-degassed Atmosphere on Its Required H–C–N–S Inventory

The aforementioned calculations in Section 3 implicitly assume that the MFI retained its MO-degassed atmosphere prior to the giant impact and that it contributed to the inventory of H–C–N–S in the BSE (Figure 1(a)). This is especially important for N, C, and H, with ∼80%, 25%, and 20% of their MFI inventory residing in the MO-degassed atmosphere, respectively (Figure 5). However, the retention of the MO-degassed atmosphere component for a Mars-sized planetary embryo for tens of millions of years prior to the giant impact is uncertain. The timing of the Moon-forming giant impact in conjunction with our current understanding on atmospheric loss rates on Mars-sized planetary embryos can be used to indirectly constrain the effect of this parameter. Hf–W chronometry, together with other isotopic systems, predicts the Moon-forming event to have occurred at timescales up to 100 Myr after CAIs (Touboul et al. 2007; Halliday 2008; Rudge et al. 2010). Numerical models predict that a Mars-sized planetary embryo rapidly loses its atmosphere when exposed to a hot surficial MO (Benedikt et al. 2020; Young et al. 2023). Since the outgassing flux approximately equals the escape rate, no stable hydrostatic equilibrium of the atmosphere can be maintained (Benedikt et al. 2020; Lammer et al. 2020). Under such conditions, the limited gravity of a Mars-sized planetary embryo cannot prevent the MO-degassed atmosphere from diffusing into space. Factors like strong X-ray and ultraviolet flux intensity of the young Sun and impact erosion would further exacerbate atmospheric loss, resulting in a complete loss of the MO-degassed atmosphere within ∼10 Myr (Erkaev et al. 2014; Schlichting et al. 2015; Woo et al. 2019)—a period concluding well before the Moon-forming event. Therefore, the MFI most likely lost its MO-degassed atmosphere during the tens of millions of years before the giant impact. This should result in a negligible contribution of the MFI's MO-degassed atmospheric component to the H–C–N–S inventory in the BSE.

Here we explore the effect of an end-member case of a complete loss of the MFI's MO-degassed atmosphere on its required H–C–N–S inventory (Figure 1(b)). In this case, the inventory of H–C–N–S in the BSE was established only by the abundances of these elements in the MFI's mantle and the fraction of its core that reequilibrated with the post-impact MO on Earth. We used this constraint in Equations (12) and (13) to determine $m_i^{whole,imp}$ for the $f = 0.1$ and $M^{MO} = 0.5M^{BSE}$ scenario. Since little S resides in the MFI's MO-degassed atmosphere (<1%; Figure 5), the required inventory of S does not vary significantly between the atmospheric loss ($C_S^{whole,imp} = 1.26$ wt%; Figure 3(b)) and the atmospheric retention ($C_S^{whole,imp} = 1.25$ wt%) cases (Figure 3(a)). As a result, the S content in the MFI's core does not vary substantially between these two cases (Figure 4). Consequently, similar to the atmospheric retention case, $D_C^{metal/silicate}$ and $D_N^{metal/silicate}$ values for S-poor cores are applicable. Given that an important fraction of the MFI's C resides in its MO-degassed atmosphere (Figure 5), the effect of atmospheric loss on its required C content is significant. The required C content in the MFI increases from 1.34 wt% for the atmospheric retention case (Figure 3(a)) to 2.23 wt% for the atmospheric loss case (Figure 3(b)). Because of the relatively high bulk C content in the MFI, the C content in its core predicted by $D_C^{metal/silicate}$ is higher than $C_{solubility}$ (Figure 4). Consequently, unlike the atmospheric retention case, the C content in the MFI's core is controlled by $C_{solubility}$, and the excess C is exsolved as graphite/diamond into the MO. Since most of the MFI's N also resides in its MO-degassed atmosphere (Figure 5), the required inventory of N for the atmospheric loss case ($C_N^{whole,imp} = 0.0883$ wt%; Figure 3(b)) is substantially higher than that of the atmospheric retention one ($C_N^{whole,imp} = 0.0021$ wt%; Figure 3(a)). Given that the MFI's MO-degassed atmosphere contains ∼10% of its entire inventory of H (Figure 5), the required inventory of H for the atmospheric loss ($C_H^{whole,imp} = 0.37$ wt%; Figure 3(b)) case is higher than the atmospheric retention ($C_H^{whole,imp} = 0.19$ wt%) case (Figure 3(a)). To summarize, in the event of a complete loss of its MO-degassed atmosphere component, the required inventories of N and C fall between those of ECs and CIs/CMs, whereas the required inventories of H are lower than

CIs/CMs and those of S are lower than both ECs and CIs/CMs. Despite the variations in the required N and S inventories with changes in f values, broadly similar conclusions can be drawn for the other scenarios explored in this study (Figure 3(b)). Note that the estimates in Figure 3(b) are on the higher end because a persistent loss of the MFI's MO-degassed atmosphere during its MO crystallization could potentially remove nearly all H, C, and N present in its mantle. This would especially limit the contribution of the MFI to the H budget of BSE because up to ∼15% of the MFI's H is present in its silicate fraction.

5. Cosmochemical Constraints on the H–C–N–S Inventory in the MFI

To assess the potential of the H–C–N–S inventory within the MFI, as constrained in Section 4, to establish the present-day abundances of these elements in the BSE, we now examine the constraints set by the meteorite record on the MFI's chemical composition. Nucleosynthetic anomalies in Ti, Cr, and Mo suggest that Earth accreted only ∼4% of materials derived from the CC reservoir, which were presumably volatile-rich (Burkhardt et al. 2021). A mixed NC–CC Mo isotopic composition of Earth implies that it accreted CC-reservoir-derived materials during the last ∼10%–20% of its growth, possibly during the Moon-forming event (Budde et al. 2019). Therefore, the maximum amount of volatile-rich, CI/CM-chondrite-like materials within the MFI can be up to 40% of its mass. For the case when the MFI lost its MO-degassed atmosphere prior to the giant impact and $M^{MO} = 0.5M^{BSE}$ and $f = 0.1$, an MFI composed of 40% CI/CM-chondrite-like materials can deliver 100%–115% of the required H, 35%–65% of the required C, 45%–85% of the required N, and 105%–170% of the required inventory of S in the BSE (Figure 6). For the other scenarios investigated in this study, similar conclusions can be drawn for H and C, whereas the contribution for N and S depends on the f value.

These results suggest that, for its most optimistic volatile inventory, i.e., accretion of 40% CI/CM-chondrite-like materials, the MFI has the potential to deliver the entire inventory of H and S and more than half the inventory of N and C, despite the limited extent of reequilibration of its core with the post-impact on Earth ($f = 0.1$) and the negligible contribution of its MO-degassed atmosphere. However, a more realistic evaluation of the volatile inventory of MFI's building blocks is required to access the validity of this optimistic scenario. The growth history of the MFI remains uncertain. While recent theoretical models suggest the growth of Mars-sized planetary embryos in the inner solar system through the accretion of a large mass of CC pebbles from the outer solar system (∼40%; Johansen et al. 2021), a low mass fraction of CC-reservoir-derived materials in Mars (∼4%), based on the isotopic signatures of several elements, implies that this growth scenario is highly improbable for the growth of planetary embryos in the inner solar system (Burkhardt et al. 2021). Instead, these planetary embryos grew through the collisional growth of smaller rocky bodies (Chambers & Wetherill 1998; Chambers 2004; Burkhardt et al. 2021). In these small rocky bodies, highly volatile elements such as H, C, and N are prone to extensive loss during thermal metamorphism and melting. For instance, a sharp drop in the bulk C and N content in chondrites with increasing peak metamorphic temperature suggests that >90% of the primitive C and N inventory is lost during heating at temperatures up to 300°C (Grewal et al. 2022a; Grewal 2022).

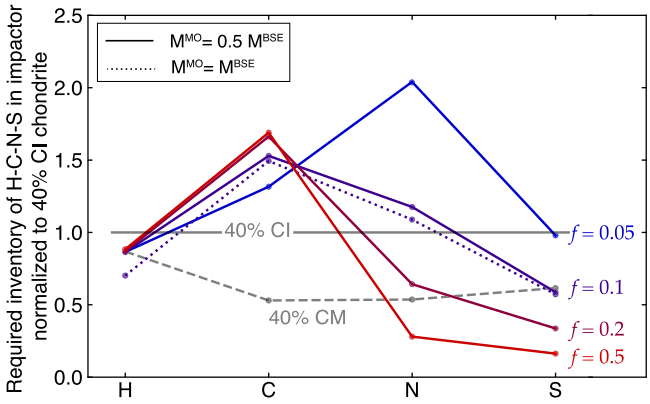

Figure 6. Comparison of the MFI's required H–C–N–S inventory to its accretion of 40% CI/CM-chondrite-like materials for the case where it lost its MO-degassed atmosphere before the giant impact. An MFI composed of 40% CI/CM-chondrite-like materials has the potential to deliver the entire required inventory of H and S and up to half of the required C, whereas its potential to deliver N depends on f values, where higher values indicate a greater potential contribution.

Similarly, low bulk C and N content in iron meteorites and low H content in primitive and asteroidal achondrites attest to substantial H–C–N loss during heating in smaller rocky bodies (Grewal et al. 2022a; Hirschmann et al. 2021; Peterson et al. 2023a, 2023b; Grewal & Asimow 2023; Newcombe et al. 2023). The impact of such volatile loss is evident in the bulk H–C–N inventory of Mars, which is estimated to contain 0.16 wt% H, 0.002 6 wt% C, and 0.000 1 wt% N (Yoshizaki & McDonough 2020). These values are significantly lower than the required H (0.37) wt%), C (2.23 wt%), and N (0.0883 wt%) inventory in the MFI. Consequently, the realistic H–C–N–S budget of the MFI prior to its atmosphere–MO–core equilibration was likely much lower than 40% CI/CM chondrite equivalent. As a result, the contribution of the MFI to the H–C–N inventory of the BSE was considerably lower than the optimistic scenarios explored in this study.

6. Establishing the Present-day Inventory of H–C–N–S in the BSE before the Moon-forming Event

Our findings suggest that for realistic estimates of its bulk H–C–N inventory, the MFI can deliver only a modest fraction of the inventory of these highly volatile elements in the BSE. Therefore, the majority of their inventory in the BSE is associated with volatile delivery either before or after the Moon-forming event. Considering its small mass (Marty 2012; Alexander 2022) and its likely differentiated nature (Bottke et al. 2010; Genda et al. 2017; Marchi et al. 2018), late accretion cannot be an important source of the less depleted atmophile elements such as H and C in the BSE. Therefore, a substantial portion of the present-day inventory of these volatiles in the BSE likely arrived prior to the Moon-forming event and managed to endure through that event.

For the volatiles present in the BSp-E to contribute to the present-day inventory of volatiles in the BSE, they must evade complete segregation into the reequilibrating fraction of the MFI's core and loss to space during the Moon-forming event. Considering that fluid dynamics models and experiments predict limited equilibration of the MFI's core with the post-impact MO (Dahl & Stevenson 2010; Deguen et al. 2014), volatiles present in the BSp-E could potentially evade segregation into the core. The participation of only a fraction of the MO in metal–silicate equilibration with the sinking emulsified metal, as predicted by

recent studies (Deguen et al. 2011, 2014), would further facilitate this. The degree of atmospheric erosion experienced by the proto-Earth during the Moon-forming event hinges on the extent of surface ground motion induced by the propagation of the shock wave during the collision (Genda & Abe 2003; Schlichting et al. 2015). Previous studies employing analytical approaches and 1D SPH simulations for head-on collisions and 3D SPH simulations for grazing collisions over a broad parameter space have demonstrated that a majority of the proto-Earth's atmosphere is retained during giant impacts, with retention rates reaching up to 90% (Genda & Abe 2003; Inamdar & Schlichting 2015; Kegerreis et al. 2020). However, if the Moon-forming event was highly energetic, it could have led to the extensive vaporization of both the proto-Earth and the MFI (Pahlevan & Stevenson 2007; Carter et al. 2020). The physics of volatile retention during such energetic events is currently underexplored and necessitates future investigation.

Before the Moon-forming event, the proto-Earth primarily grew through the stochastic accretion of differentiated planetesimals and planetary embryos (Chambers & Wetherill 1998; Morbidelli et al. 2012). Although the exact sizes of these bodies are unknown, they are expected to range from a few tens to hundreds of kilometers for planetesimals and to be Moon to Mars sized for planetary embryos (Rubie et al. 2011, 2015). Given that Moon-to-Mars-sized planetary embryos underwent collisional growth involving planetesimals, which themselves experienced volatile loss during thermal metamorphism and melting, as discussed earlier, it is anticipated that they would be depleted in volatiles relative to primitive chondritic materials. The majority of volatiles within these differentiated bodies reside either in their cores or in the MO-degassed atmospheres. Therefore, the contribution of differentiated planetesimals and planetary embryos to the volatile inventory in the BSp-E hinges on (1) the extent of reequilibration of their cores with the post-impact MOs in the growing proto-Earth and (2) the extent of atmosphere erosion during or after each impact event in the growing proto-Earth. Since atmospheric retention becomes more efficient as the proto-Earth grows to a size large enough to effectively retain atmophile elements during impacts, the present-day volatile inventory of the BSE must be biased toward the accretion of the last few planetesimals/planetary embryos before the Moon-forming event.

Alternatively, volatiles could be delivered to the proto-Earth before the Moon-forming event via a small cargo of volatile-rich, undifferentiated materials (Marty 2012; Alexander 2022). For instance, the entire inventories of H and C in the present-day BSE require the accretion of 0.001 5 M_E of CI or of 0.002 5 M_E of CM-chondrite-like materials. A modest volatile delivery by the MFI, as predicted in this study, could reduce the required mass of undifferentiated materials to lower values. Importantly, the delivery of volatiles prior to the Moon-forming event via undifferentiated materials would assist in establishing the BSE inventory of another class of highly volatile elements, namely noble gases. Due to their atmophile and lithophile characteristics, noble gases must be depleted relative to H, C, and N in the cores of differentiated planetary embryos, thereby limiting their contribution to the noble gas inventory in the BSE. Delivering atmophile elements with siderophile (H, C, and N) and lithophile (noble gases) characteristics together via volatile-rich, undifferentiated materials before the Moon-forming event provides a more straightforward solution to this problem. Establishing the BSE volatile inventory through the accretion of a small quantity of volatile-rich, undifferentiated materials before the Moon-forming event also aligns with the isotopic and dynamical constraints on the late delivery of volatile-bearing materials to Earth (Schönbächler et al. 2010; O'Brien et al. 2014, 2018; Budde et al. 2019; Steller et al. 2022).

7. Conclusions

In this study, we investigated the capacity of the MFI to establish the present-day inventory of H–C–N–S in the BSE. Using the BSE volatile inventory as a guiding constraint, we utilized inverse models to quantify the fate of H–C–N–S during atmosphere–MO–core equilibration during the post–giant impact phase on Earth. This analysis enabled us to determine the required inventory of H–C–N–S in the MFI to establish the present-day abundances of these elements in the BSE. Atmosphere–MO–core equilibration in the MFI prior to the giant impact suggests that the majority of its H–C–N–S inventory, depending on the respective metal/silicate partition coefficients ($D_i^{\mathrm{metal/silicate}}$) of these elements and their solubilities in the MOs (S_i), resides either in its core or in its MO-degassed atmosphere. With the likelihood that the MFI lost its MO-degassed atmosphere before the giant impact, the bulk of the BSE's volatiles must originate from the portion of the MFI's core that reequilibrated with Earth's post-impact MO. However, numerical models and experiments indicate that the reequilibrating portion of the impactor's core during giant impacts is small, typically around 10%. Consequently, for the MFI to independently establish the BSE's volatile inventory, it must be very volatile-rich, i.e., containing up to 50% volatile-rich CI/CM-chondrite-like materials, during its atmosphere–MO–core equilibration.

Nucleosynthetic anomalies in Mo suggest an upper limit of ~40% CC-chondrite-like materials accreted by the MFI. This implies that, for its most optimistic volatile inventory, the MFI could potentially supply the complete inventories of H and S, as well as over half of the inventories of C and N. However, as planetary embryos in the inner solar system, including the MFI, grew via the accretion of thermally metamorphosed/differentiated planetesimals, the accretion of 40% isotopically CC materials by the MFI does not directly imply that it contained 40% CI/CM-chondrite-equivalent volatiles. Consequently, the realistic contribution of MFI to the H–C–N inventory of the BSE is much lower than the optimistic scenarios explored in this study. Given the small mass added during the late accretion event, coupled with the likelihood that this event involved the addition of differentiated impactor(s), its contribution to the volatile inventory of the BSE was also limited. This suggests that a substantial portion of the present-day inventory of volatiles, especially H and C, in the BSE must have been delivered prior to the Moon-forming event and successfully survived it.

Acknowledgments

Amrita P. Vyas is thanked for improving the clarity of our communication. We thank two anonymous reviewers for their critical comments, which helped us improve several aspects of our communication. D.S.G. was supported by the start-up funds from ASU. Y.M. was supported by a Stanback Postdoctoral Fellowship from the Caltech Center for Comparative Planetary Evolution. N.X.N. was supported by the start-up funds from MIT.

ORCID iDs

Damanveer S. Grewal https://orcid.org/0000-0002-5653-1543
Yoshinori Miyazaki https://orcid.org/0000-0001-8325-8549
Nicole X. Nie https://orcid.org/0000-0003-1828-5377

References

Albarède, F. 2009, Natur, 461, 1227
Alexander, C. M. O. 2022, GeCoA, 318, 428
Armstrong, K., Frost, D. J., McCammon, C. A., Rubie, D. C., & Boffa Ballaran, T. 2019, Sci , 365, 903
Benedikt, M. R., Scherf, M., Lammer, H., et al. 2020, Icar, 347, 113772
Blanchard, I., Rubie, D. C., Jennings, E. S., et al. 2022, E&PSL, 580, 117374
Bottke, W. F., Walker, R. J., Day, J. M. D., Nesvorny, D., & Elkins-Tanton, L. 2010, Sci , 330, 1527
Bouchard, D., & Bale, C. W. 1995, MMTB, 26, 467
Boujibar, A., Andrault, D., Bouhifd, M. A., et al. 2014, E&PSL, 391, 42
Braukmüller, N., Wombacher, F., Funk, C., & Münker, C. 2019, NatGe, 12, 564
Brennan, M. C., Fischer, R. A., & Irving, J. C. E. 2020, E&PSL, 530, 115923
Budde, G., Burkhardt, C., & Kleine, T. 2019, NatAs, 3, 736
Burkhardt, C., Spitzer, F., Morbidelli, A., et al. 2021, SciA, 7, 7601
Canup, R. M. 2004, Icar, 168, 433
Canup, R. M. 2012, Sci, 338, 1052
Canup, R. M., & Asphaug, E. 2001, Natur, 412, 708
Carter, P. J., Lock, S. J., & Stewart, S. T. 2020, JGRE, 125, e06042
Chambers, J. E. 2004, E&PSL, 223, 241
Chambers, J. E., & Wetherill, G. W. 1998, Icar, 136, 304
Clesi, V., Bouhifd, M. A., Bolfan-Casanova, N., et al. 2018, SciA, 4, e1701876
Cuk, M., & Stewart, S. T. 2012, Sci, 338, 1047
Dahl, T. W., & Stevenson, D. J. 2010, E&PSL, 295, 177
Dasgupta, R., & Grewal, D. S. 2019, in Deep Carbon: Past to Present, ed. B. Orcutt, I. Daniel, & R. Dasgupta (Cambridge: Cambridge Univ. Press), 4
Dauphas, N. 2017, Natur, 541, 521
Dauphas, N., & Pourmand, A. 2011, Natur, 473, 489
Deguen, R., Landeau, M., & Olson, P. 2014, E&PSL, 391, 274
Deguen, R., Olson, P., & Cardin, P. 2011, E&PSL, 310, 303
Erkaev, N. V., Lammer, H., Elkins-Tanton, L. T., et al. 2014, P&SS, 98, 106
Fischer, R. A., Campbell, A. J., & Ciesla, F. J. 2017, E&PSL, 458, 252
Fischer, R. A., Cottrell, E., Hauri, E., Lee, K. K. M., & Le Voyer, M. 2020, PNAS, 117, 8743
Fischer, R. A., Nakajima, Y., Campbell, A. J., et al. 2015, GeCoA, 167, 177
Fischer-Gödde, M., Elfers, B.-M., Münker, C., et al. 2020, Natur, 579, 240
Fischer-Gödde, M., & Kleine, T. 2017, Natur, 541, 525
Genda, H., & Abe, Y. 2003, Icar, 164, 149
Genda, H., Brasser, R., & Mojzsis, S. J. 2017, E&PSL, 480, 25
Grewal, D. S. 2022, ApJ, 937, 123
Grewal, D. S., & Asimow, P. D. 2023, GeCoA, 344, 146
Grewal, D. S., Dasgupta, R., & Aithala, S. 2021a, E&PSL, 571, 117090
Grewal, D. S., Dasgupta, R., & Farnell, A. 2020, GeCoA, 280, 281
Grewal, D. S., Dasgupta, R., Holmes, A. K., et al. 2019a, GeCoA, 251, 87
Grewal, D. S., Dasgupta, R., Hough, T., & Farnell, A. 2021b, NatGe, 14, 369
Grewal, D. S., Dasgupta, R., & Marty, B. 2021c, NatAs, 5, 356
Grewal, D. S., Dasgupta, R., Sun, C., Tsuno, K., & Costin, G. 2019b, SciA, 5, eaau3669
Grewal, D. S., Nie, N. X., Zhang, B., Izidoro, A., & Asimow, P. D. 2024, NatAs, 8, 290
Grewal, D. S., Seales, J. D., & Dasgupta, R. 2022a, E&PSL, 598, 117847
Grewal, D. S., Sun, T., Aithala, S., et al. 2022b, GeCoA, 338, 347
Gu, J. T., Fischer, R. A., Brennan, M. C., et al. 2023, Icar, 394, 115425
Gu, J. T., Peng, B., Ji, X., et al. 2024, E&PSL, 629, 118618
Hakim, K., Spaargaren, R., Grewal, D. S., et al. 2019, AsBio, 19, 867
Halliday, A. N. 2008, RSPTA, 366, 4163
Halliday, A. N. 2013, GeCoA, 105, 146
Hirschmann, M. M. 2016, AmMin, 101, 540
Hirschmann, M. M. 2018, E&PSL, 502, 262
Hirschmann, M. M. 2022, GeCoA, 328, 221
Hirschmann, M. M., Bergin, E. A., Blake, G. A., Ciesla, F. J., & Li, J. 2021, PNAS, 118, e2026779118
Huang, D., Siebert, J., Sossi, P., et al. 2024, GeCoA, 367, 100
Ikoma, M., Elkins-Tanton, L., Hamano, K., & Suckale, J. 2018, SSRv, 214, 76
Inamdar, N. K., & Schlichting, H. E. 2015, MNRAS, 448, 1751
Jackson, C. R. M., Cottrell, E., Du, Z., Bennett, N. R., & Fei, Y. 2021, Geochem. Persp. Let., 18, 37
Johansen, A., Ronnet, T., Bizzarro, M., et al. 2021, SciA, 7, eabc0444
Kegerreis, J. A., Eke, V. R., Massey, R. J., & Teodoro, L. F. A. 2020, ApJ, 897, 161
Khan, A., Sossi, P. A., Liebske, C., Rivoldini, A., & Giardini, D. 2022, E&PSL, 578, 117330
Kuramoto, K., & Matsui, T. 1996, JGRE, 101, 14909
Kuwahara, H., Nakada, R., Kadoya, S., Yoshino, T., & Irifune, T. 2023, NatGe, 16, 461
Lammer, H., Scherf, M., Kurokawa, H., et al. 2020, SSRv, 216, 74
Landeau, M., Deguen, R., Phillips, D., et al. 2021, E&PSL, 564, 116888
Landeau, M., Olson, P., Deguen, R., & Hirsh, B. H. 2016, NatGe, 9, 786
Lherm, V., & Deguen, R. 2018, JGRB, 123, 10,496
Li, Y., Dasgupta, R., Tsuno, K., Monteleone, B., & Shimizu, N. 2016, NatGe, 9, 781
Li, Y., Wiedenbeck, M., Monteleone, B., et al. 2023, E&PSL, 605, 118032
Malavergne, V., Bureau, H., Raepsaet, C., et al. 2019, Icar, 321, 473
Marchi, S., Canup, R. M., & Walker, R. J. 2018, NatGe, 11, 77
Marty, B. 2012, E&PSL, 313-314, 56
Marty, B., Almayrac, M., Barry, P. H., et al. 2020, E&PSL, 551, 116574
Morbidelli, A., Lunine, J. I., O'Brien, D. P., Raymond, S. N., & Walsh, K. J. 2012, AREPS, 40, 251
Nakajima, M., Golabek, G. J., Wünnemann, K., et al. 2020, E&PSL, 568, 116983
Newcombe, M. E., Nielsen, S. G., Peterson, L. D., et al. 2023, Natur, 615, 854
O'Brien, D. P., Izidoro, A., Jacobson, S. A., Raymond, S. N., & Rubie, D. C. 2018, SSRv, 214, 47
O'Brien, D. P., Walsh, K. J., Morbidelli, A., Raymond, S. N., & Mandell, A. M. 2014, Icar, 239, 74
Pahlevan, K., & Stevenson, D. J. 2007, E&PSL, 262, 438
Peterson, L. D., Newcombe, M. E., Alexander, C. M. O., et al. 2023a, E&PSL, 620, 118341
Peterson, L. D., Newcombe, M. E., Alexander, C. M. O., et al. 2023b, GeCoA, 340, 141
Piet, H., Badro, J., & Gillet, P. 2017, GeoRL, 44, 11,770
Rubie, D. C., Frost, D. J., Mann, U., et al. 2011, E&PSL, 301, 31
Rubie, D. C., Jacobson, S. A., Morbidelli, A., et al. 2015, Icar, 248, 89
Rudge, J. F., Kleine, T., & Bourdon, B. 2010, NatGe, 3, 439
Rufu, R., Aharonson, O., & Perets, H. B. 2017, NatGe, 10, 89
Sakuraba, H., Kurokawa, H., Genda, H., & Ohta, K. 2021, NatSR, 11, 20894
Schlichting, H. E., Sari, R., & Yalinewich, A. 2015, Icar, 247, 81
Schönbächler, M., Carlson, R. W., Horan, M. F., Mock, T. D., & Hauri, E. H. 2010, Sci, 328, 884
Shi, L., Lu, W., Kagoshima, T., et al. 2022, NatCo, 13, 4769
Shimizu, K., Saal, A. E., Hauri, E. H., et al. 2023, GeCoA, 343, 161
Solomatov, V. 2007, in Evolution of the Earth. Treatise on Geophysics, Vol. 9, ed. G. Schubert (Amsterdam: Elsevier), 91
Sossi, P. A., Burnham, A. D., Badro, J., et al. 2020, SciA, 6, eabd1387
Sossi, P. A., Tollan, P. M. E., Badro, J., & Bower, D. J. 2023, E&PSL, 601, 117894
Speelmanns, I. M., Schmidt, M. W., & Liebske, C. 2019, E&PSL, 510, 186
Steller, T., Burkhardt, C., Yang, C., & Kleine, T. 2022, Icar, 386, 115171
Stevenson, D. J. 1990, Origin of the Earth (New York: Oxford Univ. Press), 231
Stolper, E. 1982, GeCoA, 46, 2609
Suer, T. A., Siebert, J., Remusat, L., Menguy, N., & Fiquet, G. 2017, E&PSL, 469, 84
Suer, T.-A., Jackson, C., Grewal, D. S., Dalou, C., & Lichtenberg, T. 2023, FrEaS, 11, 1159412
Sun, C., & Dasgupta, R. 2023, E&PSL, 611, 118135
Tagawa, S., Sakamoto, N., Hirose, K., et al. 2021, NatCo, 12, 2588
Touboul, M., Kleine, T., Bourdon, B., Palme, H., & Wieler, R. 2007, Natur, 450, 1206
Tsuno, K., Grewal, D. S., & Dasgupta, R. 2018, GeCoA, 238, 477
Wade, J., & Wood, B. J. 2005, E&PSL, 236, 78
Walker, R. J., Bermingham, K., Liu, J., et al. 2015, ChGeo, 411, 125
Wang, C., Hirama, J., Nagasaka, T., & Ban-Ya, S. 1991, ISIJ International, 31, 1292
Wang, Z., & Becker, H. 2013, Natur, 499, 328
Woo, J. M. Y., Genda, H., Brasser, R., & Mojzsis, S. J. 2019, Icar, 333, 87
Yoshizaki, T., & McDonough, W. F. 2020, GeCoA, 273, 137
Young, E. D., Shahar, A., & Schlichting, H. E. 2023, Natur, 616, 306
Zhou, Y., Liu, Y., Reinhardt, C., & Deng, H. 2022, AcGch, 41, 553